16th Australasian Fluid Mechanics Conference
Crown Plaza, Gold Coast, Australia
2-7 December 2007

Characterisation of a Low Reynolds Number Turbulent Boundary Layer using PIV

C.Y. Wong[1] and J. Soria[1]

[1]Laboratory for Turbulence Research in Aerospace and Combustion, Department of Mechanical Engineering (LTRAC), Monash University, Melbourne, Victoria 3800, AUSTRALIA

Abstract

An investigation by 2D-2C particle image velocimetry was carried out in the far downstream section (greater than 70 downstream boundary layer thicknesses, δ_{99} measured in the region of interest) of a nominally zero pressure gradient 0.5m-square re-circulating water tunnel seeded with 11μm Potter's hollow glass spheres. The use of a PCO4000 camera (4008 by 2672 pixel^2) in combination with a Nikon Nikkor 200mm f4 IF MF lens and a PK-13 lens extension provides a measurement spatial resolution (in the streamwise-wall normal plane) of between 2 and 25 wall units for momentum Reynolds number between 200 and 2000 respectively. The paper will present characteristic flow quantities with results from the measurements non-dimensionalised by the skin friction velocities that are estimated by the Clauser method.

Introduction

Recent research into turbulent boundary layers has concentrated on characterising and understanding their structure using various cutting-edge experimental and numerical techniques [1,2]. This work describes the use of an established digital particle image velocimetry technique to measure the stream-wise and wall-normal velocities of a naturally developing nominally zero pressure gradient low Reynolds number boundary layer in the centre plane of an experimental water tunnel. The results are compared with theory and with results from single-point measurements. Normalised velocity data ($^+$) are based on friction velocity (u_τ) calculated by the Clauser method. The aim of the paper is to characterise the LTRAC water tunnel and to examine the limitation of the DPIV technique in various regions of the boundary layer.

Experimental Details

This section describes the experimental water tunnel and the particle image velocimetry technique used in the experiments.

Experimental Facility

The experiments were conducted in the LTRAC water tunnel that has a 500mm-square cross-section with a test-section length of 5.5m. Further details of the tunnel are described in Kostas [5]. The tunnel, shown in figure 1, is a closed circuit facility and the flow is driven by a 55kW Western Electric motor coupled to a Goulds pump system. The freestream flow velocity can be adjusted in increments of 1mm/s. The maximum theoretical freestream velocity of this system is 775mm/s. However, the maximum velocity used in the present experiments is limited to 540mm/s to ensure uniformity of the freestream in the presence of a free surface. The turbulence intensity at the inlet plane was reported to be less than 1% [5] while the freestream turbulence intensity in the region of interest is measured to be just under 5%.

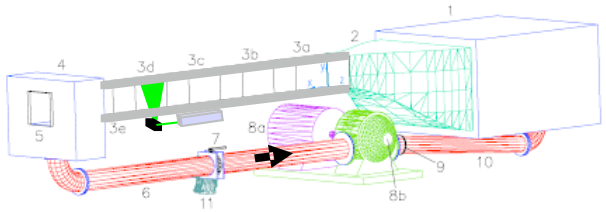

Figure 1. Schematic diagram of the horizontal closed-circuit water tunnel (adapted from Kostas 2002).

DPIV Technique

Digital Particle Image Velocimetry was used in all the experiments. A comprehensive background of the technique can be found in [7]. In summary, the technique involves the recording of particles in the field of interest by 2 singly-exposed images. Illumination of the particles by a monochromatic light source over a known time (Δt) within each recording sensor allows the spatial position of the particle images to be recorded. Knowledge of the spatial displacement of a group of particles within a given interrogation window (IW) over a known time internal allows the average velocity component to be calculated. In the present experiment, the flow was seeded with 11mm hollow glass spheres (S_g=1.1) and illumination of a 1mm thick laser sheet was provided by a pulsed Nd:YAG laser (Newwave) at a wavelength of 532nm. The particle images were recorded by a PCO.4000 camera with a spatial resolution of 4008 by 2672 pixels^2 and positioned perpendicular to the region of interest illuminated by the lightsheet. A Nikon Nikkor 200mm f/4.0 MF lens with a PK13 extension coupled to the camera enabled a fixed length-to-pixel conversion of 13.9μm/px. Since this magnification was fixed with varying Reynolds number, the typical size of measurement volumes (l^+_x, l^+_y, l^+_z) varied as follows. Increasing Re_θ increased the relative size of the interrogation volume, thus reducing spatial resolution of the PIV system.

$Re_\theta = 209 \rightarrow (0.9, 0.9, 2.2)$; $Re_\theta = 1988 \rightarrow (24, 24, 58)$.

Standard multi-grid cross-correlation algorithm was employed to process each set of PIV image pair. The experiments were optimized for an interrogation window size of 32×32 px^2 and 50% overlap between each IW. For each experimental condition, standard vector validation algorithms were used to process 420 image pairs to obtain a total of 166 by 247 vectors per image pair.

A summary of the boundary layer conditions is found in Table 1.

Re_θ	δ_{99} (mm)	δ_1 (mm) displacement	δ_2 or θ (mm) momentum	H_{12} (δ_1/δ_2)	u_τ (mm/s)	U_∞ (mm/s)
209	49.15	9.76	5.48	1.78	2.05	34.97
373	46.16	7.08	4.38	1.62	4.11	75.46
491	41.85	5.84	3.77	1.55	6.11	115.52
599	39.90	5.11	3.40	1.50	7.86	152.39
626	20.49	2.39	1.74	1.37	14.85	300.97
740	31.50	4.13	2.79	1.48	11.45	229.93
1088	29.31	3.42	2.37	1.44	18.39	382.98
1101	22.19	3.03	2.05	1.48	22.00	464.25
1190	19.41	2.76	1.87	1.48	25.16	538.43
1988	17.36	1.98	1.51	1.32	37.59	862.06

Table 1. Summary of boundary layer conditions.

Results

Effect of Spatial Resolution

In order to assess the effect of measurement volume on the experimental results, the flow case for Re_θ=1100 was fixed for two different spatial resolutions: 13.0μm/px and 17.8μm/px. These results are compared with the experimental hot-wire data of Murlis, Tsai and Bradshaw (1982) taken at Re_θ=1100, and empirical equations for turbulent boundary layer flows. Referring to Figure 2, the U^+ velocities of the 13.9μm/px case follows the trend of the theoretical curves down to y^+~20 (~0.8mm). This result is expected since the velocity gradient within the 17.8μm/px measurement volume is much steeper than the 13.0μm/px case.

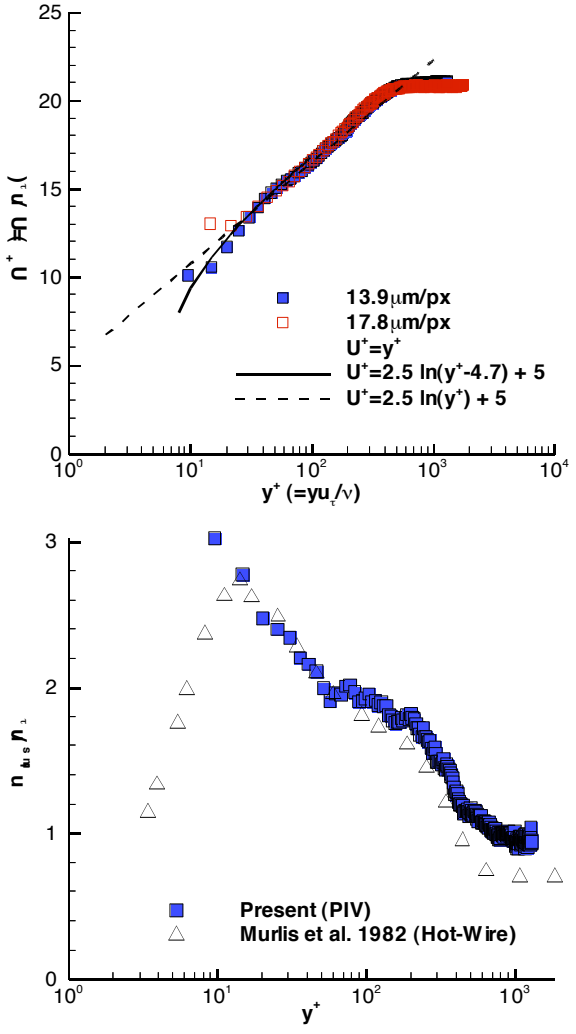

Figure 2. Effect of spatial resolution on the U^+ (Top) and u'_{rms} (Bottom) terms at Re_θ=1100.

In the $u'^+=u'_{rms}/u_\tau$ graph, a good collapse with less than 3% difference from Murlis et al's data in the region $15<y^+<60$ is observed. Interestingly, datapoints greater than $y^+=60$ consistently over-estimate the hot-wire ($l_x^+=15$) data of Murlis *et* al. (1982) from 5% at $y^+=60$ to 30% at $y^+=1070$. This may be attributed to the higher freestream turbulence intensity (~5%) for the present data compared with Murlis' data at 3.28%. Finally, the inability of the PIV system to resolve scales less than $y^+=20$ results in an over-estimation of the u'^+ data in these regions.

Mean and RMS results

In figures 3 to 5, the data in the graphs are averaged across all streamwise locations and are found to be closely self-similar at each x^+ location. For the sake of clarity, discrete data points are represented by fitting spline-fits through them. Interpretation of the results is based on the model proposed by Adrian et al. 2000.

The following empirical equations were used to model the various regions of the flow in the y-axis from the wall:

$$U^+ = y^+ \tag{1}$$

$$U^+ = \frac{1}{0.4}\ln\left(y^+ - y_0^+ + \frac{1}{0.4}\right) + 5 \tag{2}$$

$$U^+ = \frac{1}{0.4}\ln\left(y^+\right) + 5 \tag{3}$$

These equations are shown alongside the present experimental data in Figure 3. It is noted that the case at Re_θ=209 follows equation (1) fairly well down to y^+=1. On the other hand, the experimental data seem to be under-resolved for higher Re_θ numbers in the region of severe velocity gradients ($y^+<30$). This is the result of using a fixed measurement volume to measure in a boundary layer thickness decreasing with increasing Re_θ. Note also that the point of departure from the empirical equation coincides with the non-dimensional size of the measurement volume.

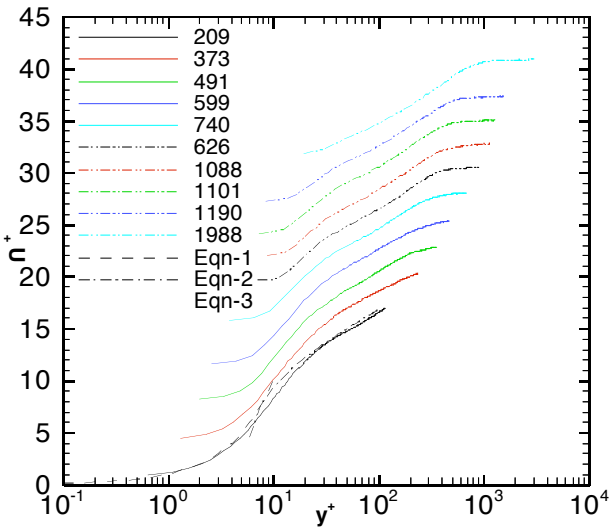

Figure 3. U^+ versus y^+ for Re_θ from 209 to 1988. Empirical solutions represented by Eqn-1, -2 and -3 are overlaid on the graph and share the same axes as Re=209. U^+ origins of all other graphs are incrementally shifted by +2 units.

Interestingly, most of the data for Re_θ<600 in the range $10<y^+<30$ do not seem to follow the graph defined by equation 2. Equation

2 consistently overestimates the experimental data. This anomaly is not likely due to insufficient spatial resolution for cases Re_θ<600. In general, data in the logarithmic region agree well with the empirical equation (Eqn 3).

Figure 4 shows the graphs for the normalised u-fluctuation (u'^+) component against the wall normal distance. The data are compared with Direct Numerical Simulation (DNS) of Spalart (1988). In general, the DNS data steadily increase to a peak of about 2.5 by y^+=15, as reported in the literature (Murlis et al., 1982; Spalart, 1988; Ching et. al, 1995). This location coincides with production events in the buffer layer. Also noteworthy is an inflexion point at around y^+=2. After the peak value of u'^+, a steady decrease occurs. This decrease is characterized by 3 inflexion points that vary with position depending on Re_θ. This suggests that, unlike the mean velocities, the fluctuating components of u beyond the viscous regime cannot be appropriately scaled by inner units.

In general, the experimental data exhibit similar peak and inflexion point characteristics as the DNS data. However, data less than y^+<10 consistently overestimate the DNS data. This is likely due to inadequate spatial resolution of the measurement volume. Despite this inadequacy, the location of the peak u-fluctuations occur at y^+~20, albeit at slightly higher values (2.6 < u'^+ <2.9). Interestingly, the DNS u'^+ peak values increase with increasing Re_θ. In contrast, the experimental u'^+ data do not provide a clear trend. Some data collapse are observed in the post-buffer region (30<y^+>100) and show no discernable trend compared with the trend of increasing y^+ with increasing Re_θ in that region. However, beyond y^+=100, there is a clear trend, for a given u'^+, that the y^+ increases with increasing Re_θ. The experimental data also show similar inflexion points similar to the DNS data post-peak. Inflexion points near to y^+~100 coincide with the location of hairpin heads and VITA (variable-interval time-averaging) events. However, the free-stream u'^+ results do not converge to zero as in the DNS data. Data collapse for y^+>30 is likewise also not observed in the experimental data.

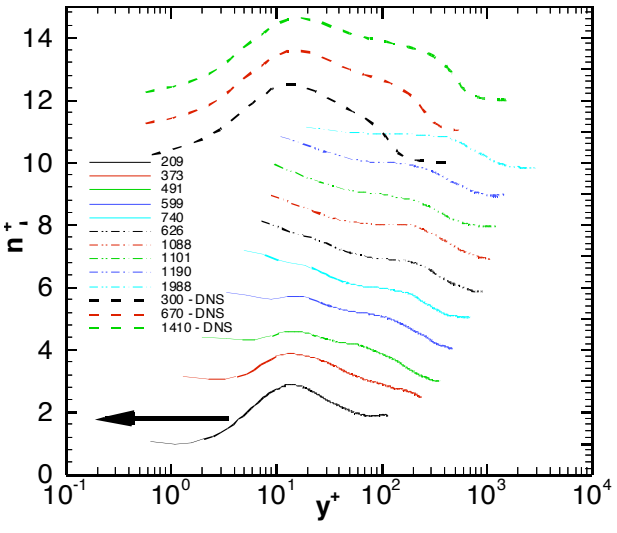

Figure 4. u'^+ versus y^+ for Re_θ from 209 to 1988. DNS solutions [from 8] for selected Re_θ are also overlaid on the same graph. Each graph is offset by +1 unit from the previous graph in the vertical axis.

Figure 5 shows the normalized v-component fluctuations (v'^+) as a function of wall normal distance. Comparable DNS data from Spalart (1988) are also shown in the figure. The experimental data largely follow the trend of the DNS graphs for regions where spatial resolution is not an issue as illustrated in Figure 2. Due to characteristic fluctuations in the water tunnel, the value of v'^+ for each case does not decrease to zero compared with the DNS data. Peaks of v'^+ are broader than u'^+ and these v'^+ peaks appear to shift to higher locations of y^+ with increasing Re_θ. Interestingly, the upturn in v'^+ value after the first peak coincides with the maximum rate of decrease in u'^+. In contrast, DNS data approach to zero in the free-stream. Again, normalization by inner variables fails to collapse data in the wake region.

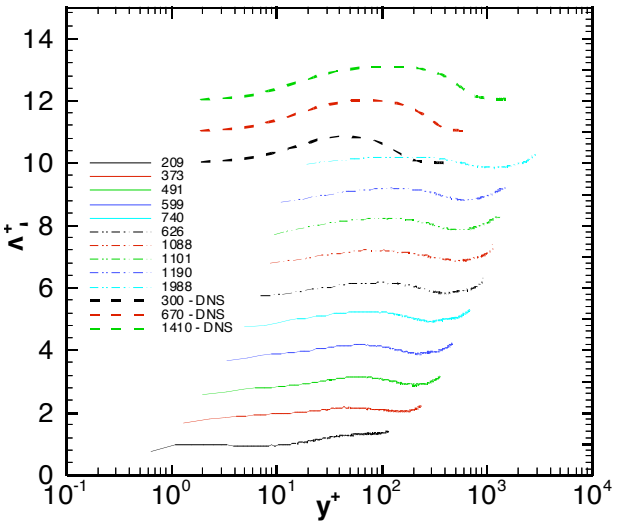

Figure 5. v'^+ versus y^+ for Re_θ from 209 to 1988. DNS solutions by [8] are also overlaid on the same graph. Each graph is offset by +1 unit from the previous graph in the vertical axis.

Conclusions

Particle Image Velocimetry experiments were conducted in a mid-tunnel region downstream of a water tunnel for a Reynolds number ranging from 209 to 1988. Characteristic u and v velocity distributions in the wall-normal direction were measured and compared with DNS data of similar Reynolds number range. In general, experimental data nearer the wall (i.e. below y+=30) were found to be sensitive to the size of the interrogation volume and over-estimates the expected magnitudes of velocities. The general shape of the experimental data graphs closely matches the DNS data in the regions where spatial resolution is not an issue. Increases in magnitudes of u' and v' towards the end of the logarithmic layer may be due to inherent fluctuations present in the water tunnel warranting further investigation.

Acknowledgments

CYW acknowledges the post-doctoral fellowship provided by an ARC discovery grant DP0663499.

References

[1] Adrian, R. J., Particle-Imaging Techniques for Experimental Fluid Mechanics, *Ann. Rev. Fluid Mech.*, **23**, 1991, 261-304.

[2] Adrian, R.J., Meinhart, C.D., Tomkins, C.D., Vortex organization in the outer region of the turbulent boundary layer, *J. Fluid Mech.*, **422**, 2000, 1-54.

[3] Ching C. Y., Djenidi L., Antonia R. A., Low-Reynolds-number effects in a turbulent boundary layer, Exp. Fluids, **19**, 1995, 61-68.

[4] Clauser, F. H., Turbulent boundary layer, In *Advances in Applied Mechanics*, **4**, 1954, 1-51.

[5] Kostas J.,*An experimental investigation of the structure of a turbulent backward facing step flow*. PhD Thesis, Laboratory for Turbulence Research in Aerospace Combustion, Department of Mechanical Engineering, Monash University Melbourne, 2002.

[6] Murlis, J., Tsai, H.M., Bradshaw, P., The structure of turbulent boundary layers at low Reynolds numbers, *J .Fluid Mech.*, **122**, 1982, 13-56.

[7] Raffel, M., Willert, C., Kompenhans, J., *Particle Image Velocimetry – A Practical Guide* Germany, Springer-Verlag, 1998.

[8] Spalart, P. R., Direct numerical simulation of a turbulent boundary layer up to R_θ=1410, *J. Fluid Mech.*, **187**, 1988, 61-98.